Title

Persistence and biodegradation of oil at the ocean floor following Deepwater Horizon

Journal

Proceedings of the National Academy of Sciences of the United States of America, 114(1)

ISSN

0027-8424

Authors

Bagby, Sarah C
Reddy, Christopher M
Aeppli, Christoph
et al.

Publication Date

2017-01-03

DOI

10.1073/pnas.1610110114

Peer reviewed

Persistence and biodegradation of oil at the ocean floor following *Deepwater Horizon*

Sarah C. Bagby[a,b], Christopher M. Reddy[c], Christoph Aeppli[d], G. Burch Fisher[e], and David L. Valentine[a,b,1]

[a]Department of Earth Science, University of California, Santa Barbara, CA 93106; [b]Marine Science Institute, University of California, Santa Barbara, CA 93106; [c]Department of Marine Chemistry and Geochemistry, Woods Hole Oceanographic Institution, Woods Hole, MA 02543; [d]Bigelow Laboratory for Ocean Sciences, East Boothbay, ME 04544; and [e]Jackson School of Geosciences, University of Texas at Austin, Austin, TX 78712

Edited by Donald E. Canfield, Institute of Biology and Nordic Center for Earth Evolution, University of Southern Denmark, Odense M., Denmark, and approved November 20, 2016 (received for review June 22, 2016)

The 2010 *Deepwater Horizon* disaster introduced an unprecedented discharge of oil into the deep Gulf of Mexico. Considerable uncertainty has persisted regarding the oil's fate and effects in the deep ocean. In this work we assess the compound-specific rates of biodegradation for 125 aliphatic, aromatic, and biomarker petroleum hydrocarbons that settled to the deep ocean floor following release from the damaged Macondo Well. Based on a dataset comprising measurements of up to 168 distinct hydrocarbon analytes in 2,980 sediment samples collected within 4 y of the spill, we develop a Macondo oil "fingerprint" and conservatively identify a subset of 312 surficial samples consistent with contamination by Macondo oil. Three trends emerge from analysis of the biodegradation rates of 125 individual hydrocarbons in these samples. First, molecular structure served to modulate biodegradation in a predictable fashion, with the simplest structures subject to fastest loss, indicating that biodegradation in the deep ocean progresses similarly to other environments. Second, for many alkanes and polycyclic aromatic hydrocarbons biodegradation occurred in two distinct phases, consistent with rapid loss while oil particles remained suspended followed by slow loss after deposition to the seafloor. Third, the extent of biodegradation for any given sample was influenced by the hydrocarbon content, leading to substantially greater hydrocarbon persistence among the more highly contaminated samples. In addition, under some conditions we find strong evidence for extensive degradation of numerous petroleum biomarkers, notably including the native internal standard 17α(H),21β(H)-hopane, commonly used to calculate the extent of oil weathering.

Deepwater Horizon | biodegradation | oil spills | hydrocarbon | petroleum biomarkers

On 20 April 2010, a blowout from the Macondo Well in the Gulf of Mexico (GOM) caused an explosion on the *Deepwater Horizon* (DWH) mobile offshore drilling unit that ultimately led to its sinking and the deaths of 11 crewmembers. From the time of the blowout until the well was capped on 15 July 2010, petroleum fluids flowed continuously from the Macondo Well, with environmental emission estimates of 4.1 million barrels of oil and 1.7×10^{11} g natural gas (1–3). The spill was noteworthy not only for its volume but also for its distance offshore and its depth: Oil and gas entered the ocean at a water depth of ∼1,500 m and then partitioned between the deep ocean and the sea surface. This partitioning may have varied over time because of reservoir depressurization and deliberate interventions such as the shearing of the riser pipe and the application of chemical dispersant at the wellhead (4–6). In all, approximately half of the oil ascended to the ocean surface (1, 7), where it was skimmed or flared by response teams, trapped in sinking particles by marine oil snow sedimentation and flocculent accumulation (8, 9), washed ashore, or left exposed to the canonical weathering processes of evaporation, biodegradation, and photooxidation (7, 10). The rest remained in the deep ocean. Because the DWH event was the first major spill to occur in the deep ocean, the processes determining the fate of this oil were largely unknown.

In the wake of the spill, water-column data shed light on the physical partitioning of the submerged oil. Many compounds containing <10 carbon atoms (e.g., natural gas, benzene and its alkylated analogs, cycloalkanes, and branched alkanes) dissolved in seawater to form deep, aqueous plumes (2, 6, 11–16); in the first weeks of the spill, dissolution is also expected to have influenced the distribution of two- and three-ring polycyclic aromatic hydrocarbons (PAHs), particularly naphthalene and its alkylated analogs, and to a lesser extent fluorene, phenanthrene, and anthracene and their alkylated analogs. Hydrocarbons that remained undissolved became trapped in the deep ocean in a suspension of small (less than ∼100 μm) droplets of liquid oil that lacked the buoyant force to rise through the water column. These droplets remained concentrated close to the well's coordinates (2, 11, 12, 15), but modeling suggests that droplet size drove further vertical partitioning, with droplets >50 μm mixing upwards by August 2010 and smaller droplets remaining suspended in the deep ocean (7, 17, 18). Some suspended oil was eventually deposited to the seafloor, likely via oil–mineral aggregates or microbial flocs (8, 19, 20), with intense contamination within ∼5 km of the well (21–26). Surficial sediments near the well were found to carry >1,000-fold–elevated concentrations of dioctyl sodium sulfosuccinate (4), an active ingredient of the chemical dispersant applied at the wellhead, and to exhibit a radiocarbon deficit consistent with oil deposition (27). We recently identified a 3,200-km^2 deposition footprint stretching southwest from the wellhead (28). This footprint, marked by substantial heterogeneity in the oil mass of deposited particles, was estimated to account for ∼4–31% of the submerged oil (28).

Significance

The *Deepwater Horizon* event led to an unprecedented discharge of ∼4.1 million barrels of oil to the Gulf of Mexico. The deposition of ∼4–31% of this oil to the seafloor has been quantified previously on a bulk basis. In this work, we assess the extent of degradation over 4 y postspill for each of 125 petroleum hydrocarbons that contaminated the seafloor. As expected, chemically simpler compounds broke down more quickly than complex compounds, but degradation rates also depended on environmental context: Breakdown often was faster before seafloor deposition than after and for oil trapped in small droplets than for oil in large particles. These results provide a basis to predict the long-term fate of seafloor oil.

Author contributions: S.C.B., C.M.R., C.A., and D.L.V. designed research; S.C.B. and G.B.F. performed research; S.C.B., G.B.F., and D.L.V. analyzed data; and S.C.B., C.M.R., C.A., G.B.F., and D.L.V. wrote the paper.

The authors declare no conflict of interest.

This article is a PNAS Direct Submission.

Freely available online through the PNAS open access option.

Data deposition: All raw data analyzed in this article are publicly available via the Natural Resource Damage Assessment website (https://dwhdiver.orr.noaa.gov/explore-the-data/). The cleaned and filtered dataset, together with all analysis code used in the paper and a README file describing the use of the code, has been bundled with all necessary R packages to make a functional research compendium. This compendium has been deposited with Figshare, with the DOI 10.6084/m9.figshare.4001262.

[1]To whom correspondence should be addressed. Email: valentine@geol.ucsb.edu.

This article contains supporting information online at www.pnas.org/lookup/suppl/doi:10.1073/pnas.1610110114/-/DCSupplemental.

Superimposed on these changes in physical distribution, hydrocarbons trapped in the deep ocean were subject to biologically mediated loss processes (i.e., biodegradation) (12, 16, 18, 29–31). For sparingly soluble hydrocarbons, biodegradation is expected to serve as the primary cause of weathering in the deep ocean because other key weathering processes (e.g., evaporation, photooxidation) depend on atmospheric and solar exposure. Although hydrocarbon recalcitrance to biodegradation is expected to scale roughly with molecular mass and steric complexity (32), the rates at which specific hydrocarbons are metabolized vary based on myriad environmental variables: temperature, salinity, pressure, oxygen concentration, pH, solar exposure, availability of nutrients and other sources of organic matter (33), water availability, access to substrate, solid-phase interactions, competition, predation, and inhibition (34). Although early reports addressed the degradation of some low- to moderate-molecular-mass compounds in the water column (12, 14, 16), the degradation rates of the petroleum hydrocarbons constituting Macondo oil after seafloor deposition are unknown. However, it is these rates, and the factors that control them, that will largely determine the long-term fate and biological impacts of the spill on the GOM seafloor.

In this work we address the fate of oil that was deposited on the floor of the deep ocean following the DWH event. We use publicly available data from the Natural Resource Damage Assessment (NRDA) process to identify samples contaminated by oil from the Macondo Well conservatively and to analyze the rate and extent of biodegradation for 125 hydrocarbon compounds spanning 4 y postspill. Based on the results, we identify key factors that modulated biodegradation, finding that a dependence on the intensity of contamination overlaid the expected trends in chemical structure and complexity.

Results

Identification of Macondo-Contaminated Samples. In previous work, we established that surficial GOM sediments not contaminated with Macondo oil typically bear <75 ng/g of the native internal standard 17α(H),21β(H)-hopane and that the large majority of contamination lies within 40 km of the wellhead, in a footprint extending southwest from the wellhead (28). However, this region is also the site of ongoing natural seepage, and inclusion of any seeped oils could severely distort analysis of the time course of seafloor Macondo oil weathering. Thus, the first goal in our analysis was to identify a subset of NRDA samples in which the detected petroleum hydrocarbons originate unambiguously from the Macondo Well.

This task is complicated by there being no "smoking gun" compound that is present in Macondo Well oil but absent from local seeps. Nonetheless, the relative abundances of the suite of recalcitrant native petroleum compounds commonly referred to as "biomarkers" constitute a chemical fingerprint for Macondo Well oil. We used 12 diagnostic biomarker ratios capturing a broad range of these compounds' structural diversity to develop an aggregate Macondo dissimilarity index (hereafter, MDI), as detailed in the *SI Appendix*, *SI Text*. The spatial structuring of MDI fingerprint results (Fig. 1 and *SI Appendix*, Fig. S2), particularly the appearance of distinct patterns of biomarker ratios deeper in the sediment column where seep oil is expected to be the dominant source (25, 26), suggests that the matching process successfully identified samples contaminated by Macondo oil against a low-level background of chemically distinct seep oils.

Of the 2,980 sections of sediment cores collected in the NRDA sampling effort (*SI Appendix*, *SI Text*), 443 matched the MDI fingerprint and hereafter are referred to as "Macondo-contaminated samples." However, these samples originated from sediment depths of up to 5 cm. Although spilled oil may be pushed downcore in the course of sampling, it also can be mixed downward in sediment by bioturbation in situ (35), exposing it to different oxygen concentrations and microbial communities for an unknown period. To reduce heterogeneity in the dataset, we exclude all samples with upper depth ≥0.5 cm from further consideration, yielding a conservative final set of 312 samples of Macondo-contaminated surficial sediments.

These samples were collected at 272 stations in the course of 14 cruises from September 2010 to June 2014, at seafloor depths ranging from 1,029 to 1,912 m (median, 1,494 m; interquartile range, 1,394–1,568 m). Notably, only ∼5% of these Macondo-contaminated samples were collected at depths consistent with "bathtub ring" deposition by deep plumes impinging on the continental slope, and ∼95% lie within the deeper, more heavily contaminated fallout plume (Fig. 1). The contamination in this region has previously been shown to derive from oil from the deep plume rather than from oil that rose to the surface, weathered, and sank again to the seafloor (28). In that work, we established 28 ng/g as the mean background concentration of hopane in surficial sediments ≥40 km from the wellhead; 97% of surficial sediments sampled at this distance from the well contained <75 ng/g hopane. In the Macondo oil–contaminated surficial sediments we identify here with the MDI, hopane concentrations range from 43.8 to 14,100 ng/g, indicating a >320-fold range in the severity of contamination. Among the petroleum hydrocarbons measured in these samples, we identified a set of 125 aliphatic compounds, PAHs, and polycyclic isoprenoid and triaromatic sterane petroleum biomarkers with sufficiently high data quality (*SI Appendix*, *SI Text*) to permit kinetic analysis. The resulting dataset comprises 34,769 measurements, a median of 310 measurements per compound.

Initial Observations of Hydrocarbon Weathering Kinetics. To begin our analyses of these compounds, we used hopane as an internal standard, first normalizing each analyte concentration to the hopane concentration in that sample (36, 37) and then normalizing that ratio to the corresponding ratio in source oil. We refer to these doubly normalized values as the "fraction remaining" of a given compound. On initial examination of single-compound datasets, we observed what appeared to be a contamination-level dependence in the change in fraction remaining over time (*SI Appendix*, Fig. S3*A*). To test this apparent pattern, we binned samples by hopane concentration (low, <400 ng/g; moderate, 400–750 ng/g; high, ≥750 ng/g) as a proxy for contamination level and asked whether the distribution of fraction-remaining data differed significantly ($P < 0.05$, Kolmogorov–Smirnov test) across bins (*SI Appendix*, Fig. S3 *B* and *C*). We found significant differences between the low- and high-contamination bins for 94% of the compounds and significant differences between the low- and moderate-contamination bins for 60% of the compounds. This result raises the strong possibility that oil-particle size influences weathering rates, perhaps because of the relatively limited bioavailability of oil in large particles, oxygen or nutrient drawdown within large particles, or distinct deposition histories for different particle-size classes. In light of this result, we assessed biodegradation rates separately for the low-, moderate-, and high-contamination bins. We had sufficient data (*Methods*) to analyze 353 (of a possible 372) compound–contamination bin datasets.

To a first approximation, biodegradation is expected to follow simple exponential decay kinetics from a starting point of fraction remaining = 1 at t_0. However, each particle of deposited oil has weathered in two distinct physical environments, first in suspension and then on the seafloor, with considerable differences in key environmental variables including advection, temperature, oxygen and nutrient concentration, pressure, and, potentially, microbial community abundance and composition. Thus, we considered the possibility that the best fit might be a biphasic (broken-stick) model, with independent decay rates in the two phases. It should be noted that, with sediment and source-oil data only, we have end-members for the first phase of such a model, but we lack direct measurements to define the trajectory of that phase. Initial loss could have obeyed first-order kinetics or a more complex trajectory—e.g., a rapid physical process associated with discharge,

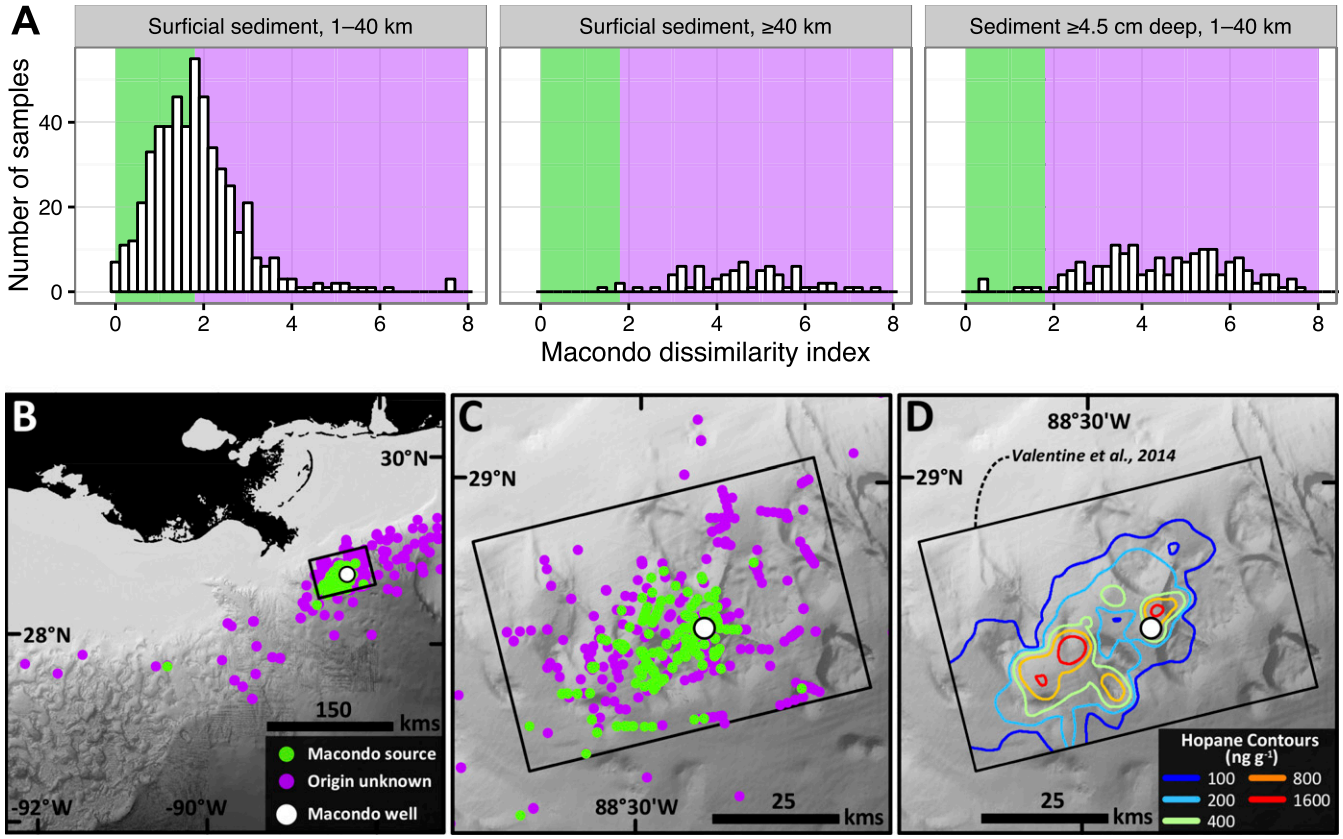

Fig. 1. Application of the MDI to NRDA sediment samples. (*A*) Spatial distribution of MDI values. (*Left*) Surficial sediments (upper depth = 0 cm) collected 1–40 km from the wellhead. (*Center*) Surficial sediments collected ≥40 km from the wellhead. (*Right*) Downcore sediments (upper depth ≥4.5 cm) collected 1–40 km from the wellhead. Samples falling in the green region (MDI <1.8) are consistent with Macondo oil. (*B*) Bathymetric chart of the region around the wellhead showing MDI results for each sample collected. Green symbols, MDI <1.8; purple symbols, MDI ≥1.8. (*C*) Zoomed view of *B* showing detail in the immediate vicinity of the wellhead. (*D*) Footprint of seafloor oil deposition in the immediate vicinity of the wellhead as detected by hopane-concentration anomalies in previous work (28).

followed by biodegradation and/or dissolution from suspended particles. As a third possibility, we considered a simple exponential decay model in which the *y* intercept was allowed to vary freely.

Because oil continued to flow from the wellhead for 87 d, there is a large intrinsic uncertainty in the length of time a given particle of deposited oil was exposed to weathering before sample collection. To cope with this uncertainty explicitly, for each analyte at each contamination level, we generated 100 pseudoreplicate datasets with different randomized time offsets of 0–87 d added to each data point. We fit our three models to each pseudoreplicate, using the Bayesian information criterion (BIC) to choose the best fit, and we report the median of best-fit predictions.

To assess the global quality of our fits, we examined the so-called "pull" distribution, i.e., the distribution of (fitted slope)/(error on fit) (38). The high tails in these distributions, most notably at low and moderate contamination levels, indicate a pathology in the hopane-normalized dataset (*SI Appendix*, *SI Text* and Fig. S4). High pull values were especially common among aliphatic compounds of at least 29 carbons, compounds that, when normalized to hopane, appear to show increasing fraction remaining over time (*SI Appendix*, Fig. S4 *D* and *E*). The simplest explanation for this behavior is that hopane is not, in fact, conservative for these conditions but rather is more labile than the most recalcitrant aliphatics and aromatics.

Such hopane lability is not unusual. Substantial hopane degradation has been observed before in laboratory settings (39) and in other environments; studying the OSSA II spill in the Bolivian Altiplano, Douglas et al. (40) found that the long-chain alkane *n*-C40 provided a more conservative basis for normalization than hopane. The longest-chain aliphatic present in Macondo oil at sufficient concentrations to be useful for normalization is octatriacontane, *n*-C38. Accordingly, we renormalized our data to *n*-C38 concentrations and repeated our analysis. (To avoid confusion, we continue to categorize samples as showing low, moderate, or high contamination using the bins established above.) The resulting pull distributions were far less distorted (*SI Appendix*, Fig. S4*B*), indicating that normalization to *n*-C38 offered a far more reliable basis for fitting than normalization to hopane. In the remainder of this work we refer exclusively to analysis of *n*-C38–normalized concentration data.

Factors Controlling Seafloor Hydrocarbon Weathering Rates. We performed 35,300 head-to-head model comparisons (100 pseudoreplicates for each of 353 datasets), finding strong statistical support (ΔBIC ≥6) for any model in just under half the comparisons (17,115). Strikingly, the biphasic (broken stick) model was the best-fit model in every such case. Extensive early loss was far more common among pseudoreplicates best fit by the biphasic model than among those best fit by the single-phase models (*SI Appendix*, Fig. S5). The biphasic model was disproportionately likely to be the best-fit model in the low- and moderate-contamination bins and among aliphatic and aromatic compounds (*SI Appendix*, Fig. S5). A subset of data and fits is presented in *SI Appendix*, Fig. S6.

These results are consistent with a model in which all compounds are subject to two phases of weathering, but the transition between phases is obscured when the first phase is either retarded by chemical recalcitrance or low diffusivity or is limited by large particle size. Particle size could influence first-phase weathering either

through bioavailability, in that hydrocarbons trapped in larger particles could be comparatively inaccessible to oil-degrading microbes, or through deposition dynamics, e.g., if larger particles tended to be deposited more rapidly, after less exposure to the plume's comparatively favorable conditions for biodegradation. Because the earliest samples in the sediment dataset were collected 160 d postexplosion, we cannot distinguish between these possibilities.

Hydrocarbon molecular mass and structure typically influence biodegradation rates, with progressively slower degradation with increasing molecular mass, ring number, and alkyl branching (32, 34, 41–44). We tested the validity of these relationships for the seafloor by comparing the residual fraction for each hydrocarbon remaining in the sediment 4 y after the spill began. Among the compounds examined, carbon skeletons range from nine to 37 atoms (aliphatics, 9–37; aromatics, 9–22; biomarkers, 23–35) and vary in complexity from the straight-chain aliphatic *n*-C9 to the pentacyclic, multiply substituted biomarker pentakishomohopane. This analysis provides an unparalleled window into the disposition of oil following the DWH event, in that the extent of biodegradation is quantified simultaneously for 125 petroleum hydrocarbons across wide-ranging contamination levels. The results of this analysis clearly show the influence of molecular mass and structure on the extent of biodegradation (Fig. 2, Table 1, and *SI Appendix*, Table S1).

Among straight-chain aliphatic compounds, the extent of degradation after 4 y changes sharply at chain lengths of 28 or 29 carbons (Fig. 3 and Table 1). Among longer chains, across all contamination levels, the fraction remaining after 4 y increases steadily with chain length, reaching 100% for *n*-C37; by contrast, degradation is almost entirely complete for shorter chains (Fig. 3 and Table 1). Indeed, shorter-chain compounds are largely lost by 160 d at low and moderate contamination levels; at high contamination levels, the loss of these compounds at 160 d is substantial but far from complete (*SI Appendix*, Fig. S7). Branching of the carbon backbone is expected to slow biodegradation (32); this effect is not detectable in the light- and moderate-contamination bins, but at high contamination levels the branched compounds show significantly less biodegradation (24–62% contamination remaining) by 160 d postexplosion than their straight-chain counterparts (6–33%). Even in these highly contaminated samples, the degradation of branched-chain aliphatics is largely complete by 4 y postexplosion (Figs. 2 and 3).

Among aromatic compounds, chemical complexity begins to retard biodegradation at lower molecular masses (Figs. 4 and 5, Table 1, and *SI Appendix*, Table S1). At low and moderate levels of contamination, biodegradation is largely complete by 160 d for compounds of <16 or 17 carbons but not for larger compounds (Table 1 and *SI Appendix*, Figs. S8 and S9). Postdeposition biodegradation is detectable for most larger compounds at low and moderate levels of contamination (low contamination: 19 of 21 compounds; moderate contamination: 13 of 21 compounds). At high contamination levels, the largest compound for which biodegradation is nearly complete (<5% remaining) by 160 d is the 14-carbon PAH phenanthrene, and only half of the smaller compounds are degraded to <5% remaining by 160 d (*SI Appendix*, Figs. S8 and S9). Although postdeposition biodegradation is detectable for 15

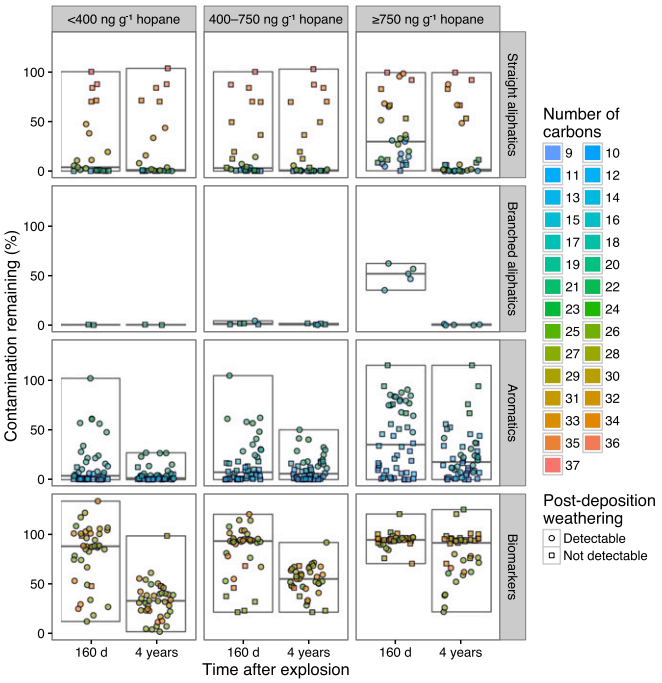

Fig. 2. Overview of the relationship between carbon skeleton size and structure and the extent of biodegradation at 160 d and 4 y postexplosion. Symbols are colored by the number of carbons in the skeleton; symbol shape indicates whether postdeposition biodegradation was or was not detectable for each compound. Results are the median of 100 pseudoreplicate fits for each compound–contamination bin dataset.

Table 1. Size-dependent differences in persistence of aliphatic and aromatic compounds

		Percent remaining after 160 d				Percent remaining after 4 y			
Class	Hopane, ng/g	Boundary position*		Among smaller analytes	Among larger analytes	Boundary position*		Among smaller analytes	Among larger analytes
Aliphatics	<400	C28	Median	0.6	70.2	C29	Median	0.4	70.8
			Range	0.1–5.5	11.2–100.4		Range	0.1–3.7	15.8–103.8
	400–750	C28	Median	1.1	69.8	C28	Median	0.5	69.8
			Range	0.1–7.2	12.5–100.3		Range	0.1–3.6	12.5–103
	≥750	C13	Median	6.1	36.5	C29	Median	0.6	74.8
			Range	0.4–17.5	6.2–99.5		Range	0–11.4	48.5–99.5
Aromatics	<400	C17	Median	0.5	26.2	C20	Median	0.9	23.3
			Range	0–6.5	7.1–102.3		Range	0–12.6	15.3–26.9
	400–750	C16	Median	1.2	28.7	C16	Median	1.2	18.3
			Range	0.1–12.5	6.5–105.1		Range	0.1–12.5	6.5–50.4
	≥750	C14	Median	5.1	75.1	C14	Median	5.1	24.9
			Range	0.1–44.2	11.9–115.5		Range	0.1–44.2	7.3–115.5

*Boundary position is the number of carbons below which loss is so extensive that no trend in percent remaining vs. carbon number can be distinguished and above which there is a clear size trend in percent remaining. The boundary between these regimes can be seen most clearly in Fig. 3 and *SI Appendix*, Fig. S7, where the y axes are ordered by carbon number. Higher chemical lability and lower contamination levels favor more extensive biodegradation, pushing the boundary between regimes to larger carbon numbers.

of 32 larger aromatic compounds at high contamination levels, none of these compounds is degraded to <5% remaining by 4 y postexplosion (Figs. 4 and 5 and Table 1). High contamination also highlights the pattern of relatively fast loss of unsubstituted parent PAHs and slower loss of alkylated daughter PAHs (Figs. 4 and 5 and *SI Appendix*, Figs. S8 and S9).

The largest and most complex hydrocarbons analyzed are the biomarkers: polycyclic isoprenoids including hopanes and diahopanes, terpanes, and steranes and diasteranes, as well as triaromatic steranes. As discussed above, our initial analysis of hopane-normalized data pointed to some degree of biomarker weathering. As analysis of *n*-C38–normalized data makes clear, the large majority of biomarkers analyzed are subject to biodegradation on the timescale studied, consistent with previous observations of Macondo oil in slicks, oiled sands, and deep-sea corals (Fig. 6 and *SI Appendix*, Table S1) (45–47). Biodegradation is limited in all contamination bins before deposition (*SI Appendix*, Fig. S10; median predictions at 160 d: low contamination, 89% remaining; moderate contamination, 94% remaining; high contamination, 95% remaining) but is extensive in the low- and moderate-contamination bins after deposition (median predictions at 4 y: low contamination, 33%; moderate contamination, 56%; high contamination, 92%). For biomarkers, we find no clear relationship between carbon number and degradation rate (Figs. 2 and 6), likely because some of the larger biomarkers (e.g., homohopanes) bear relatively labile alkyl chain substituents (45).

Although these findings are consistent with established biodegradation patterns, they contradict the biodegradation trends reported by Hazen et al. in early analysis of water-column samples (12). Their work suggested half-lives of 0.6–9.5 d for alkane compounds in suspended oil, with no discernible trend related to molecular mass or methyl branching. The discrepancy between that work and the results obtained here led us to reanalyze the dataset they studied. We find two significant shortcomings in their analysis. First, although they set out to determine biodegradation rates within the deep plume of oil, the depth of the plume varied from place to place. By using all samples collected at water depths of 1,099–1,219 m, regardless of station, they included numerous samples collected outside local concentration peaks. Because hydrocarbon concentration dropped sharply above and below the plume, inclusion of these out-of-plume samples introduced a low bias to the resulting half-lives. Second, heightening this bias, they analyzed raw concentration data, without normalizing to the concentration of a conservative compound. Analysis of normalized, in-plume data for the alkanes studied by Hazen et al. (12) (*SI Appendix*, Fig. S11) reveals half-lives 10-fold to ~50-fold longer than previously reported values (*SI Appendix*, Fig. S12). We find no evidence for the extraordinarily rapid, structure-independent degradation rates originally reported.

Discussion

Dissimilarity Fingerprinting Advances Deep-Sea Oil Spill Forensics. Although a Macondo fingerprint for use in oily samples has been developed recently (48), the MDI fingerprint developed for this work represents a significant forensic advance for the study of the DWH spill in sediments. Our approach is independently supported by the good spatial agreement found between the deposition footprint as defined by the MDI and the footprint as previously defined by hopane (28) and natural abundance radiocarbon (27) anomalies. The MDI offers an advantage over these methods in its ability to distinguish between seeped and spilled oil in individual samples: Among sediment samples that do not meet our MDI threshold, a distinct and coherent fingerprint emerges at greater distances from the Macondo Well and lower depths in the sediment column, likely representing weathered oil that originated in natural seeps. This sensitivity suggests that comparable dissimilarity approaches may be useful for analysis of future spills.

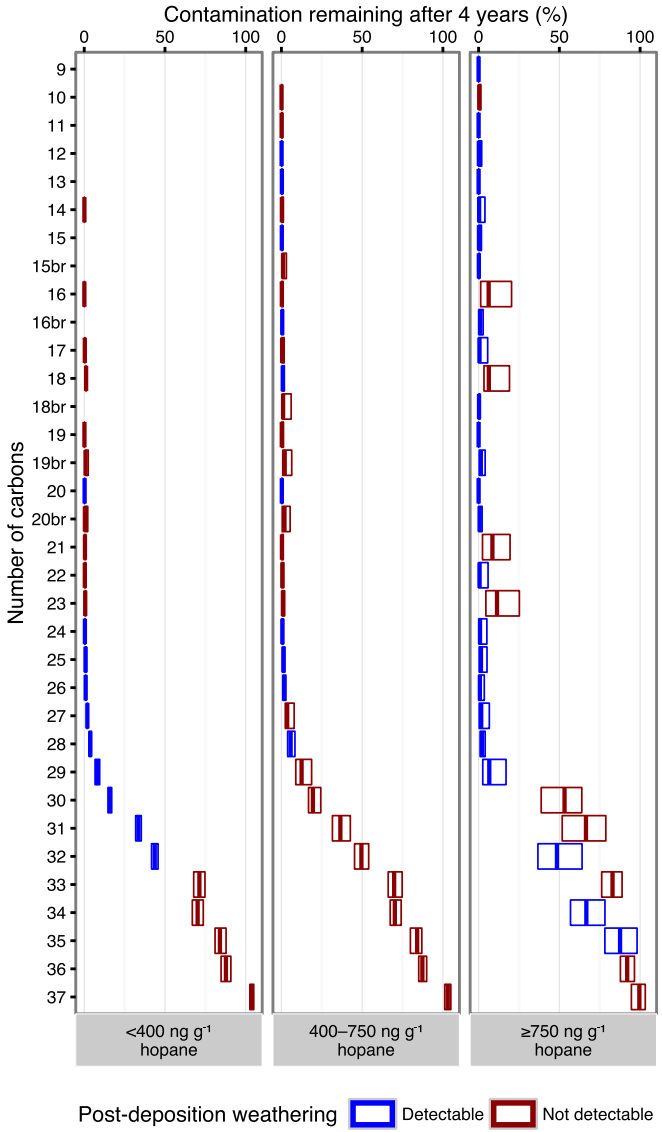

Fig. 3. Percent of aliphatic compounds remaining at 4 y postexplosion, ordered by chain length. Branched compounds are indicated by "br" on the *y* axis. Compounds for which biodegradation was detectable after deposition are shown in blue, with crossbars indicating the fitted value and boxes indicating the 95% confidence interval (CI) of the median fit result. Compounds for which postdeposition biodegradation was not detectable are shown in red, with vertical bars indicating the median and boxes indicating the interquartile range of measured values.

In light of the degradation of biomarkers described above, it is reasonable to ask on what timescale a biomarker-based fingerprint can remain diagnostic. Starting with Macondo oil, we calculated the projected time-course changes in the ratios used to calculate MDI (*SI Appendix*, Fig. S13). We find that in sediments with low contamination the MDI as described here should remain useful for ~5.4 y; it should remain useful for ~10 y in moderately contaminated sediments and for ~5 y in highly contaminated sediments. Notably, the biomarkers whose loss causes the MDI to drift over time differ across contamination levels: Steranes dominate the loss of discrimination at low contamination levels, hopanes at moderate contamination levels, and triaromatic steranes at high contamination levels (*SI Appendix*, Fig. S13*B*). Although the MDI's useful lifetime might be extended by relaxing the threshold to account for drift or by modifying the chosen set of biomarker ratios

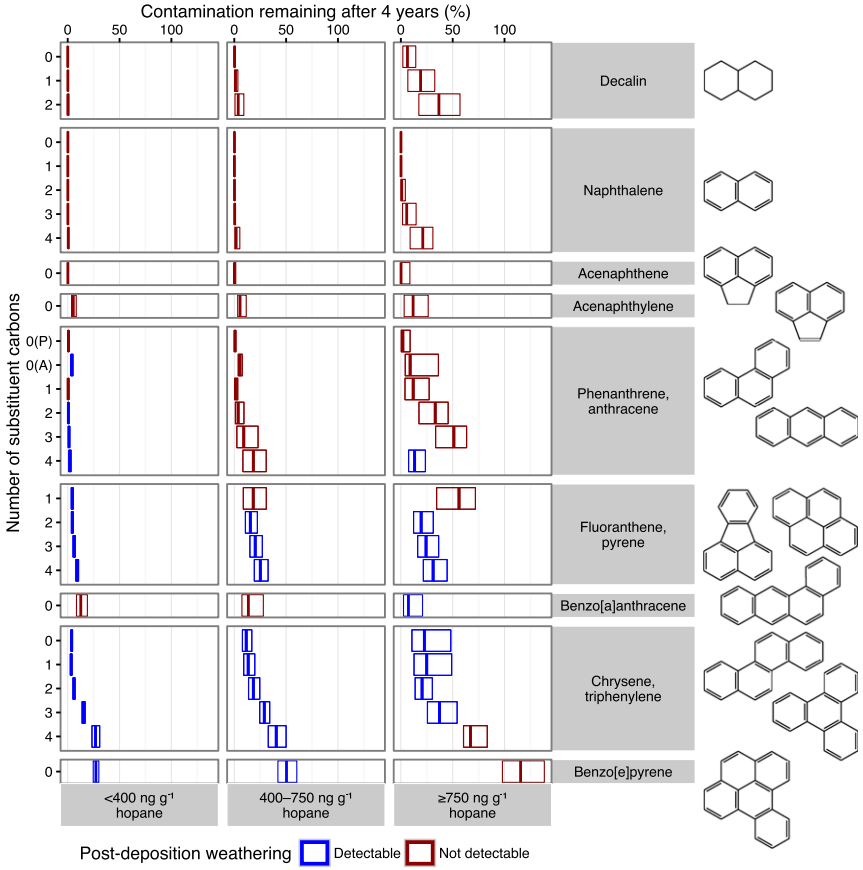

Fig. 4. Percent remaining of aromatic compounds with six-membered rings 4 y postexplosion. (Decalin is not aromatic but is included here.) Panels are ordered by increasing carbon skeleton size from top to bottom and within each panel by increasing number of carbon substituents. Where multiple carbon skeletons are shown for a single group at right, the compounds in that category were not separately resolved in chemical analysis, unless otherwise indicated on the *y* axis. 0(P), unsubstituted phenanthrene only; 0(A), unsubstituted anthracene only. Compounds for which biodegradation was detectable after deposition are shown in blue, with crossbars indicating the fitted value and boxes indicating the 95% CI of the median fit result. Compounds for which post-deposition biodegradation was not detectable are shown in red, with vertical bars indicating the median and boxes indicating the interquartile range of measured values.

(45), these changes would likely come at the cost of increasing false positives.

Pseudoreplicates Can Address Uncertainties in Weathering. Although Monte Carlo methods are common in other fields, they have not typically been used in oil-spill assessment. Here, we used ensembles of pseudoreplicates with added noise in the time coordinate to address a major uncertainty in the dataset: For the oiled particle(s) collected in each sediment sample, how much time elapsed between wellhead emission and sample collection? Although many spills are contained far more quickly than the DWH event, no oil spill is without its uncertainties. We can increase our confidence in our analyses of these events and set bounds on the range of possible outcomes by modeling the uncertainties explicitly.

Hopane Is Not Always Conserved. For more than 20 y, hopane has been widely used as a conservative internal standard (36, 37) for quantification of oil weathering after spills. Indeed, we have previously treated hopane as conservative and have used the seafloor hopane anomaly as a basis to calculate the corresponding contamination burden as ∼4–31% of the oil from the deep plume (28). The analysis we present here supports the conclusion that hopane does not behave uniformly as a conservative biomarker in Macondo oil deposited to the seafloor but rather undergoes significant biodegradation at low and moderate contamination levels. Two-thirds of the surficial samples identified by the MDI fall into the low-contamination class, and for these samples only 39% of hopane remained at 4 y postexplosion. An additional 19% of samples fall into the moderate-contamination class; in these samples, 64% of hopane remained after 4 y. However, hopane is relatively persistent (95% remaining after 4 y) in the highly contaminated samples, supporting its use a conservative marker in heavily contaminated environments. These results add to other studies (39, 40, 49, 50) that redefine views on hopane's fidelity and utility as an internal standard. In light of the research community's crucial public role in assessing the damage wrought by past and future spills, this mounting evidence strongly suggests that best practices are due for revision. Although the use of some internal standard is essential, hopane should not be assumed to be the best choice for timescales of months to years but rather should be assessed for utility on a case-by-case basis.

In this spirit, we have updated our previous hopane-based estimate of seafloor oil contamination from the DWH event (28). Working within the same 3,200-km^2 study area considered in that study (28), we applied the most robust kriging model identified there [empirical Bayesian kriging (EBK) model EBK-C] to (*i*) *n*-C38 concentrations and (*ii*) projections of original hopane concentration. The resulting interpolated deposition footprints are in good agreement, accounting for, respectively, ∼13.7 and <14.7% of the oil from the deep plume. The comparatively small disparity between these estimates and the previous EBK-C estimate of ∼12% (28) likely results from the freshness of samples used in interpolation (collected ≤1.5 y postexplosion) and from the recalcitrance of hopane in heavily contaminated samples.

Multiple Factors Control Biodegradation of Macondo Oil. The contamination-level bins used in the present work were chosen empirically, based on exploratory analysis of the fraction-remaining data. It is noteworthy, then, that these bins correspond neatly to the level of contamination expected from the different particle-size classes suggested by previous modeling work (28). Contamination with <400 ng/g hopane is consistent with the deposition of a single oiled particle from the smallest predicted size class (∼0.024 g oil); contamination with ≥750 ng/g hopane is consistent with the deposition of more than one particle of the larger classes. We observed more scatter in the fraction-remaining data in the 400–750 ng/g

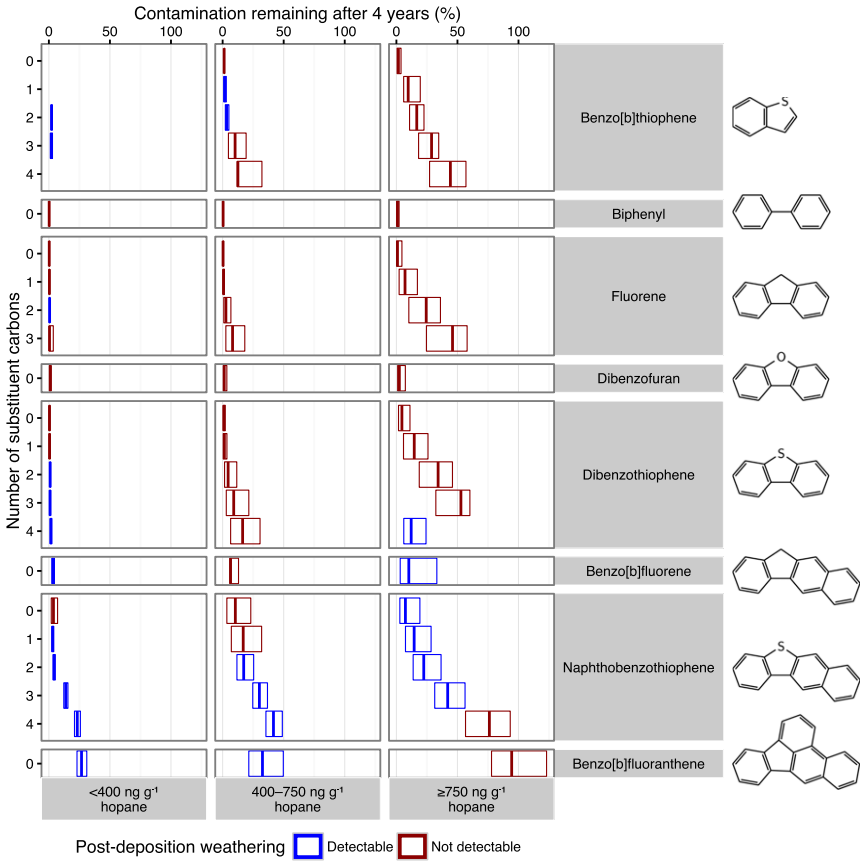

Fig. 5. Percent of aromatic compounds with five-membered rings remaining 4 y postexplosion. (Biphenyl is included here because of its structural resemblance to fluorene, dibenzofuran, and dibenzothiophene.) Panels are ordered by increasing carbon skeleton size from top to bottom and within each panel by increasing number of carbon substituents. Compounds for which biodegradation was detectable after deposition are shown in blue, with crossbars indicating the fitted value and boxes the 95% CI of the median fit result. Compounds for which postdeposition biodegradation was not detectable are shown in red, with vertical bars indicating the median and boxes the interquartile range of measured values.

hopane bin than in either the <400 ng/g or the ≥750 ng/g hopane bins; this moderate-contamination level can arise either from two or three particles of the smallest size class or from one of the particles in the low tail of the second size class. The observed kinetic heterogeneity therefore might reflect a mixture of light- and heavy-contamination–like behaviors across different samples. Alternatively, particles in this concentration range may represent two populations deposited on the seafloor with different histories.

The effect of contamination level on the biodegradation rate reported here is consistent with reports from other environmental settings [e.g., the boulder armoring that protected oil from biodegradation following the *Exxon Valdez* disaster (51), beach sands (52), and bioremediation studies as reviewed previously (53)]. Notably, however, previous examples of this phenomenon have all involved larger spatial scales and higher concentrations. The contamination effect we observe suggests that a similar phenomenon also operates on the approximately millimeter scale and within oil volumes of ∼0.01–1 mL (28).

Contra Hazen et al. (12), and consistent with independent metatranscriptomic evidence (54), we find clear evidence for the expected relationship between chemical size and complexity and biodegradation rate. This relationship is clearest in the aliphatic and aromatic compounds analyzed and is most obscure among the biomarkers. The observed rates of diasterane biodegradation are particularly variable, consistent with previous observations in salt marshes (46). This variability is also consistent with previous observations (45, 47), and the observed concentration dependence provides a framework for interpreting such variable sterane deficits.

The robust distinction between the two phases of loss for samples with low and moderate contamination suggests that controls on weathering differed before and after deposition. We hypothesize that this effect arises from a relatively rapid microbial response to freshly suspended oil droplets followed by a marked reduction in microbial metabolism after droplets aggregated and settled to the sea floor, where biodegradation might be limited by insufficient access to a terminal oxidant or nutrients. Among highly contaminated samples, predeposition biodegradation could be limited either by the faster deposition of larger particles, limiting their exposure to in-plume weathering conditions, or by larger particles' low surface area:volume ratio, limiting bioavailability. In the latter case, particles might spread upon deposition, allowing biodegradation to proceed.

Two limitations of the biphasic kinetic model should be emphasized. First, the distribution of deposition times, i.e., of breakpoints between phases, is not known. We chose to fix the breakpoint uniformly at t = 160 d postexplosion because that represents the earliest date from which we have Macondo-contaminated sediment samples. The modal breakpoint could be earlier, and, as noted above, could differ for different particle-size classes. Second, the first phase of degradation is characterized only by its modeled endpoints, i.e., source oil and the earliest sediment samples. Complex kinetics could lurk in the first phase; we can make claims only about the total extent of biodegradation before seafloor deposition, not about the time-dependence of biodegradation in this window.

Stout and Payne (25) have recently argued that the predominant signals in DWH sediment chemistry data are distance-related: The farther from the well an oily particle was deposited, the greater is the extent of biodegradation. They hypothesize that biodegradation proceeds more rapidly in suspension than after sedimentation, so that hydrocarbons in oily particles that were carried further (and thus remained in suspension longer) are systematically more degraded than those in particles deposited closer to the wellhead. This model is consistent with our finding that the majority of pseudoreplicates are best fit by a two-phase biodegradation model, with faster degradation before deposition.

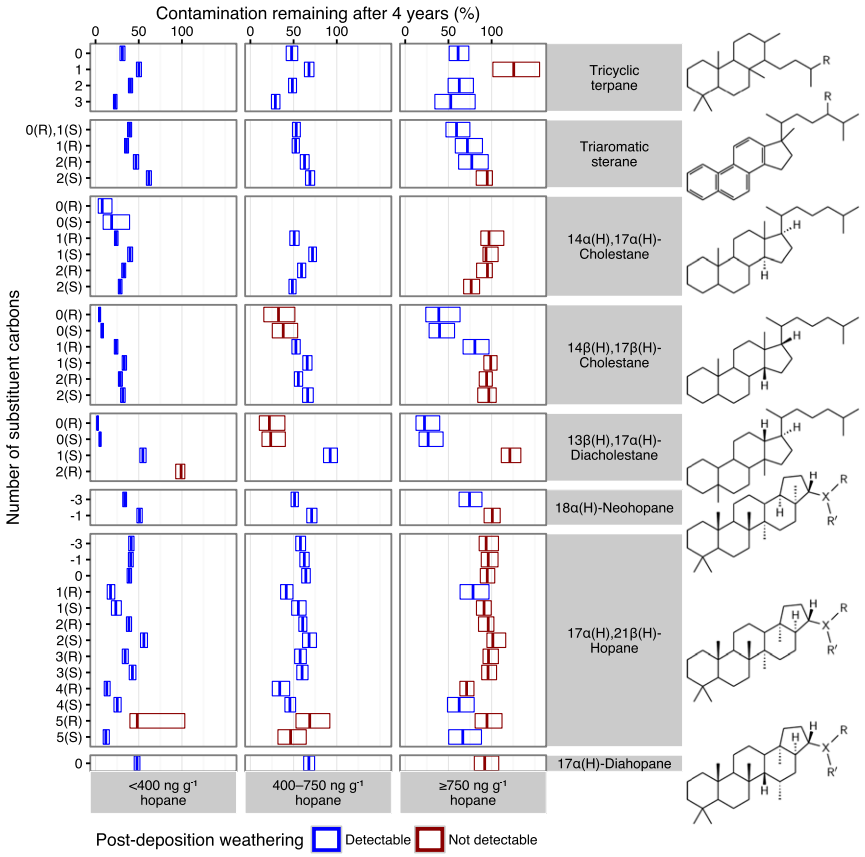

Fig. 6. Percent of biomarker compounds remaining 4 y postexplosion. Panels are ordered by increasing carbon skeleton size from top to bottom and within each panel by increasing number of carbon substituents, with (R) and (S) substituent stereochemistry displayed separately. Among neohopanes and hopanes, –3 indicates the tris-nor compounds and –1 indicates the nor compounds; 1(R) and 1(S) through 5(R) and 5(S) indicate homohopanes through pentakishomohopanes. Compounds for which biodegradation was detectable after deposition are shown in blue, with crossbars indicating the fitted value and boxes indicating the 95% CI of the median fit result. Compounds for which postdeposition biodegradation was not detectable are shown in red, with vertical bars indicating the median and boxes indicating the interquartile range of measured values.

In light of the variability of currents in the region (29) and the unknown deposition history of oiled particles in different samples, our analysis does not account explicitly for distance from the wellhead; the breakpoint between the first and second phase of biodegradation is treated as constant for all samples. Thus, if a distance signal exists, it should be detectable in the residuals of our fits: Macondo-contaminated samples collected farther from the wellhead should have systematically more negative residuals (i.e., greater degradation than the model predicts, occurring during the longer-than-average time to deposition) than Macondo-contaminated samples collected closer to the wellhead. To check, we examined the relationship between model residuals and distance from the wellhead, limiting the analysis to pseudoreplicates with at least moderate support (ΔBIC $\geq$2) for the best-fit model.

We found a significant negative slope in all contamination bins for aliphatic and aromatic compounds. The more recalcitrant biomarkers show a smaller negative slope at low contamination levels, a negligible negative slope at moderate contamination levels, and a negligible positive slope at high contamination levels (*SI Appendix*, Fig. S14). This result is consistent with our observation that two-phase kinetics dominate for aliphatic and aromatic compounds but not for biomarkers: The length of time spent in suspension should matter more when the difference between pre- and postdeposition rates is larger. An additional nuance is that the distance effect is weakest whenever predeposition biodegradation is either very fast or very slow. This diminution in distance effect could reflect a Goldilocks effect: For labile compounds in small particles, even those deposited closest to the well remained in suspension for multiple degradation half-lives, whereas for recalcitrant compounds in large particles, even those deposited farthest were in suspension for only one or two. Both cases should damp the distance signal.

Implications for Response Efforts in Future Deep Spills. Future spill-response efforts may be informed by two key findings from the present work: first, that biodegradation is much faster in suspension than after deposition for most compounds studied; and second, that contamination level is a key control on degradation rates. These findings suggest that the lasting benthic impact of deep-sea spills may be minimized by measures that drive oil to stay suspended in smaller droplets for longer—an intended mode of action of the 2.9×10^6 L of chemical dispersant applied directly at the wellhead during the spill. While it is not known to what extent dispersant drove oil into microdroplets that biodegraded while remaining suspended in the ocean's interior, the identification of the dispersant's active ingredient in the deep ocean intrusion layers (6) and in benthic oil deposits (4) suggests that the dispersant did remain in suspension with the oil. Furthermore, roller-tank experiments with Macondo oil (19) demonstrated that dispersant delayed the formation of marine snow, perhaps through a direct influence on the surface-layer properties of oil particles or an effect on the microbial release of aggregation-promoting exudates. Together with the present findings, these observations suggest that subsea dispersant application contributes to a net acceleration of biodegradation.

However, other lines of evidence cloud this picture. A recent study questions the efficacy of the subsea dispersant application in modulating droplet size (55), and the variable impacts of dispersant on biodegradation are at the center of an ongoing debate (56, 57). The effect of dispersant itself on the benthos is not well understood, but components of dispersant have been found to persist in sediments and in fragile deep-sea coral communities on a scale of years (4). Decisions regarding the use of dispersant in future spills thus need to weigh not only endpoint hydrocarbon concentration but also context: The net environmental impact of years-long exposure to high local concentrations of undispersed sediment-bound oil may

or may not be more severe than the combined effects of short-term exposure of the deep water column to microdroplets of oil and dispersant and long-term exposure of sediments to their residues.

Conclusions

Our compound-specific analysis confirms expected chemical structure trends in biodegradation rates but holds several surprises: First, that biomarkers, including hopane, are subject to substantial biodegradation after deposition; second, that biodegradation patterns differ markedly depending on the extent of contamination; and third, that biodegradation was typically much faster in the short window while oil particles remained suspended than it was subsequently on the deep seafloor. These results provide a basis for predicting the ongoing biodegradation of Macondo oil on the floor of the Gulf of Mexico, inform the ongoing debate about the merits of subsea dispersant use, and argue for caution when using hopane as an internal standard for oil-spill research at long timescales.

Methods

Data used in this work are freely available from the National Oceanic and Atmospheric Administration (NOAA), as part of the NRDA of the DWH event. Data were downloaded from the NRDA data site, now at https://dwhdiver.orr.noaa.gov/explore-the-data/, and included all chemistry data in the sediment category through 8 May 2015 and all chemistry data in the subsurface sediment, oil, and water categories as of 2 May 2014. All data used in this study are included in the research compendium deposited with Figshare (https://figshare.com), DOI 10.6084/m9.figshare.4001262. Bathymetric data were downloaded 11 June 2014 from the NOAA GEODAS server (www.ngdc.noaa.gov/mgg/gdas/gd_designagrid.html); xyz values are from the ETOPO1 dataset (https://www.ngdc.noaa.gov/mgg/global/global.html) at 1-min resolution.

Analysis was performed in R (v. 3.3.1), using the packages broom (v. 0.4.1), e1071 (v. 1.6-7), NADA (v. 1.5-6), survival (v. 2.39-5), geosphere (v. 1.5-5), sp (v. 1.2-3), lubridate (v. 1.5.6), assertr (v. 1.0.2), reshape2 (v. 1.4.1), dplyr (v. 0.5.0), tidyr (v. 0.6.0), plyr (v. 1.8.4), and marmap (v. 0.9.5). Figures were produced in R with packages png (v. 0.1-7), Cairo (v. 1.5-9), extrafont (v. 0.17), gridExtra (v. 2.0.1), hexbin (v. 1.27.1), cowplot (v. 0.6.2), scales (v. 0.4.0), and ggplot2 (v. 2.1.0). All code used in the analysis is deposited with the Figshare compendium (DOI 10.6084/m9.figshare.4001262).

Data Reduction. We filtered the dataset to remove all stations with seafloor depth of less than 200 m, all samples identified as "Filter/Particulate," and all bottom-water samples. See *SI Appendix, SI Text* for a complete description of sample curation. We included only analyses with reported quality codes of Not Available, J, and U. Analyses with quality code U were censored as the interval [0, detection limit (dl)], even where the reported concentration exceeded the dl. For analyses with quality code J, concentrations were censored as the interval (0, dl) in the small number of cases ($n = 149$ in the full dataset, $n = 2$ remaining in the final dataset) where the reported concentration fell below the reported dl and were uncensored otherwise. Analyses with quality code Not Available were uniformly treated as quantitative, i.e., uncensored.

Some samples had been measured repeatedly at different calibration scales, often yielding a nondetect at high dl and a quantitative result at low dl. In these cases, the nondetects were excluded from further analysis. In some cases, a single physical sample was split for multiple measurements of an analyte using different analytical methods, with one method marked by Alpha Analytical as disfavored and flagged with an "X" suffix in the labrep. We discarded these analyses (*SI Appendix, SI Text*). Methods that the NRDA later designated as disfavored were the only methods used to analyze the 40 biomarker compounds in 256 samples ($n = 13$ in the final dataset) collected within 8 mo of the explosion. Because few or no other data were available for these compounds in this period (*SI Appendix*, Fig. S15), we included these measurements in our analysis. Comparison fits excluding these measurements indicated that these data points did not skew the results (*SI Appendix, SI Text* and Figs. S16 and S17).

Identification of Macondo Oil by the MDI. We assessed 83 biomarker ratios (45, 58) for inclusion in the MDI score, choosing 12 based on their data completeness, discriminating ability, and chemical diversity (*SI Appendix*, Table S2). We defined a set of reference samples (*SI Appendix*, Table S3) consisting of (*i*) the 11 samples (pooling physical splits) from study name Chem–Source Oil 2010 and (*ii*) the 12 samples identified in the NRDA Sediment and Subsurface datasets at <1 km from the wellhead, upper depth 0 cm, and hopane ≥750 ng/g (i.e., ≥10-fold above background), collected <1 y after the spill midpoint. This composite source was chosen to account for potential variability in the measured biomarker ratios of Macondo oil such as might be caused by changes in fluid composition during discharge, matrix effects impacting extraction from sediment, and analytical uncertainty. We defined a per-ratio dissimilarity metric (*SI Appendix, SI Text*, Eq. S1) and calculated the MDI as the average penalty over n informative (noncensored) ratios (*SI Appendix, SI Text*, Eq. S2). We excluded samples with $n < 8$ from further analysis. See *SI Appendix, SI Text* and Fig. S1 for details of the choice of the cutoff value MDI <1.8.

Data Normalization and Contamination Binning. To control for differences in absolute oil mass, we analyzed biodegradation kinetics in terms of the concentration of each compound remaining in a sample relative to the concentration of an internal reference compound and normalized that ratio to the corresponding ratio in Macondo Well (MW) source oil (*SI Appendix, SI Text*). The result is the fraction remaining: for an analyte a, $F_{a,samp} = (C_{a,samp}/C_{ref,samp})/(C_{a,MW}/C_{ref,MW})$. Samples for which the measurement of the reference compound was censored were excluded from further analysis.

As reference compounds for normalization, we considered both the biomarker hopane, expected to be recalcitrant, and *n*-C38, the longest detectable aliphatic compound. We calculated the pull for each pseudoreplicate as the best-fit slope divided by the fitted error on the slope and examined the positive arm of the pull distributions for each contamination level and compound class (*SI Appendix, SI Text* and Fig. S4). Pull SDs were calculated as the rms of positive pull values (*SI Appendix, SI Text*). After examination of the skewed pull distributions (*SI Appendix*, Fig. S4) resulting from fitting hopane-normalized data, we proceeded with analysis of *n*-C38–normalized data instead. See *SI Appendix, SI Text* for complete description of data normalization.

Visual inspection of fraction-remaining time-course plots suggested a systematic influence of contamination level on fraction remaining. We used the two-sample Kolmogorov–Smirnov test to compare empirical cumulative distribution functions across contamination bins (low, <400 ng/g hopane; moderate, 400–750 ng/g hopane; high, ≥750 ng/g hopane), finding significant differences ($P < 0.05$) for the large majority of compounds. We applied these contamination bins to all further analysis.

Construction and Head-To-Head Comparison of Fits. We attempted to fit all 353 compound–contamination bin datasets that include ≥10 uncensored data points and ≤80% censored observations. Three low-contamination datasets [13β(H),17α(H)-20R-ethyldiacholestane and the 20R and 20S enantiomers of 14α(H),17α(H)-cholestane] spanned a time range of <100 d in sediment (samples collected at 160–239 d postexplosion). All other datasets spanned >200 d in sediment, with 337 of the 353 datasets spanning ~3.5 y. Because the dataset includes nondetects, we fit using maximum likelihood-based survival analysis (R package survival), assuming a Gaussian distribution for the log-transformed response variable.

For each dataset, we fit 100 pseudoreplicates with uniformly distributed noise added to the time axis to reflect the 87-d uncertainty in time from emission to sampling. We used the BIC to perform head-to-head comparisons of three models on each pseudoreplicate's log-transformed fraction-remaining data: a single-phase linear model with the y intercept permitted to vary freely; a single-phase linear model with the y intercept fixed at 0; and a piecewise-linear (broken-stick) biphasic model with breakpoint fixed at 160 d after the explosion. For the biphasic model, the first phase is constrained only by its endpoints, i.e., source oil at t = 0 and the earliest sediment samples at t = 160 d. For each pseudoreplicate, we identified the best-fit model as the model that minimized the BIC. See *SI Appendix, SI Text* for details of extracting predictions from pseudoreplicate ensembles.

EBK Estimation of Seafloor Oil Contamination Burden. To revise our estimate of the seafloor contamination burden, we repeated the EBK process used in ref. 28 with the most robust model from that analysis, there designated EBK-C. To facilitate comparison, we used the same set of 534 samples here as in our previous work, with the exception that 14 of the samples had no concentration data available for *n*-C38. The exclusion of these points from the original hopane analysis had no net effect on the previously published contamination burden. To calculate the excess *n*-C38 in the footprint area, we used a background concentration of 82 ng/g *n*-C38, calculated as the mean *n*-C38 concentration in surficial sediment samples that pass our quality filters, have an MDI >1.8, and were collected ≥40 km from the wellhead. For the EBK-C run using projected hopane concentrations in unweathered oil, we assumed the maximum possible age for the oil at the time of sampling (i.e., that all oil collected had emerged from the wellhead on the day of the explosion). For each sample that matched the Macondo fingerprint, we used the median best-fit model from the appropriate contamination bin to calculate the mass of hopane that would have been present in that sample absent biodegradation. Hopane concentrations from samples with an MDI ≥1.8 were

held constant. As in ref. 28, we calculated the excess hopane burden using a background concentration of 28 ng/g hopane.

ACKNOWLEDGMENTS. We thank Elizabeth Porta (Alpha Analytical) for useful advice, Deborah French-McCay (Applied Science Associates) for preparation and coordination of NRDA cruises, and the crew and scientists of the 18 NRDA cruises whose sediment samples we analyzed. This work was supported, in part, by National Science Foundation Grants OCE-1333162, OCE-0961725, EAR-0950600, and OCE-1046144 (to D.L.V.) and OCE-1333148 (to C.M.R.) and by Simons Foundation Grant 385324 (to D.L.V.).

1. McNutt MK, et al. (2012) Review of flow rate estimates of the Deepwater Horizon oil spill. *Proc Natl Acad Sci USA* 109(50):20260–20267.
2. Reddy CM, et al. (2012) Composition and fate of gas and oil released to the water column during the Deepwater Horizon oil spill. *Proc Natl Acad Sci USA* 109(50): 20229–20234.
3. Camilli R, et al. (2012) Acoustic measurement of the Deepwater Horizon Macondo well flow rate. *Proc Natl Acad Sci USA* 109(50):20235–20239.
4. White HK, et al. (2014) Long-term persistence of dispersants following the Deepwater Horizon oil spill. *Environ Sci Technol Lett* 1(7):295–299.
5. Socolofsky SA, et al. (2015) Intercomparison of oil spill prediction models for accidental blowout scenarios with and without subsea chemical dispersant injection. *Mar Pollut Bull* 96(1-2):110–126.
6. Kujawinski EB, et al. (2011) Fate of dispersants associated with the Deepwater Horizon oil spill. *Environ Sci Technol* 45(4):1298–1306.
7. Ryerson TB, et al. (2012) Chemical data quantify Deepwater Horizon hydrocarbon flow rate and environmental distribution. *Proc Natl Acad Sci USA* 109(50): 20246–20253.
8. Passow U, Ziervogel K, Asper V, Diercks A (2012) Marine snow formation in the aftermath of the Deepwater Horizon spill in the Gulf of Mexico. *Environ Res Lett* 7(3): 035301.
9. Daly KL, Passow U, Chanton J, Hollander D (2016) Assessing the impacts of oil-associated marine snow formation and sedimentation during and after the Deepwater Horizon oil spill. *Anthropocene* 13:18–33.
10. Aeppli C, et al. (2012) Oil weathering after the Deepwater Horizon disaster led to the formation of oxygenated residues. *Environ Sci Technol* 46(16):8799–8807.
11. Diercks A-R, et al. (2010) Characterization of subsurface polycyclic aromatic hydrocarbons at the Deepwater Horizon site. *Geophys Res Lett* 37(20):L20602.
12. Hazen TC, et al. (2010) Deep-sea oil plume enriches indigenous oil-degrading bacteria. *Science* 330(6001):204–208.
13. Joye SB, MacDonald IR, Leifer I, Asper V (2011) Magnitude and oxidation potential of hydrocarbon gases released from the BP oil well blowout. *Nat Geosci* 4(3):160–164.
14. Kessler JD, et al. (2011) A persistent oxygen anomaly reveals the fate of spilled methane in the deep Gulf of Mexico. *Science* 331(6015):312–315.
15. Spier C, Stringfellow WT, Hazen TC, Conrad M (2013) Distribution of hydrocarbons released during the 2010 MC252 oil spill in deep offshore waters. *Environ Pollut* 173: 224–230.
16. Valentine DL, et al. (2010) Propane respiration jump-starts microbial response to a deep oil spill. *Science* 330(6001):208–211.
17. Lindo-Atichati D, et al. (2016) Simulating the effects of droplet size, high-pressure biodegradation, and variable flow rate on the subsea evolution of deep plumes from the Macondo blowout. *Deep Sea Res Part II Top Stud Oceanogr* 129:301–310.
18. North EW, et al. (2015) The influence of droplet size and biodegradation on the transport of subsurface oil droplets during the Deepwater Horizon spill: A model sensitivity study. *Environ Res Lett* 10(2):024016.
19. Passow U (2014) Formation of rapidly-sinking, oil-associated marine snow. *Deep-Sea Res PT II* 129:232–240.
20. Stoffyn-Egli P, Lee K (2002) Formation and characterization of oil–mineral aggregates. *Spill Sci Technol Bull* 8(1):31–44.
21. Montagna PA, et al. (2013) Deep-sea benthic footprint of the Deepwater Horizon blowout. *PLoS One* 8(8):e70540.
22. Liu Z, Liu J, Zhu Q, Wu W (2012) The weathering of oil after the Deepwater Horizon oil spill: Insights from the chemical composition of the oil from the sea surface, salt marshes and sediments. *Environ Res Lett* 7(3):035302.
23. Liu Y, MacFadyen A, Ji Z-G, Weisberg RH, eds (2011) *Monitoring and Modeling the Deepwater Horizon Oil Spill: A Record-Breaking Enterprise* (American Geophysical Union, Washington, DC), 10.1029/GM195.
24. Kimes NE, et al. (2013) Metagenomic analysis and metabolite profiling of deep-sea sediments from the Gulf of Mexico following the Deepwater Horizon oil spill. *Front Microbiol* 4:50.
25. Stout SA, Payne JR (2016) Macondo oil in deep-sea sediments: Part 1 - sub-sea weathering of oil deposited on the seafloor. *Mar Pollut Bull* 111(1-2):365–380.
26. Stout SA, Payne JR, Ricker RW, Baker G, Lewis C (2016) Macondo oil in deep-sea sediments: Part 2 - Distribution and distinction from background and natural oil seeps. *Mar Pollut Bull* 111(1-2):381–401.
27. Chanton J, et al. (2015) Using natural abundance radiocarbon to trace the flux of petrocarbon to the seafloor following the Deepwater Horizon oil spill. *Environ Sci Technol* 49(2):847–854.
28. Valentine DL, et al. (2014) Fallout plume of submerged oil from Deepwater Horizon. *Proc Natl Acad Sci USA* 111(45):15906–15911.
29. Valentine DL, et al. (2012) Dynamic autoinoculation and the microbial ecology of a deep water hydrocarbon irruption. *Proc Natl Acad Sci USA* 109(50):20286–20291.
30. Redmond MC, Valentine DL (2012) Natural gas and temperature structured a microbial community response to the Deepwater Horizon oil spill. *Proc Natl Acad Sci USA* 109(50):20292–20297.
31. Dubinsky EA, et al. (2013) Succession of hydrocarbon-degrading bacteria in the aftermath of the deepwater horizon oil spill in the gulf of Mexico. *Environ Sci Technol* 47(19):10860–10867.
32. Gros J, et al. (2014) Resolving biodegradation patterns of persistent saturated hydrocarbons in weathered oil samples from the Deepwater Horizon disaster. *Environ Sci Technol* 48(3):1628–1637.
33. Slater GF, White HK, Eglinton TI, Reddy CM (2005) Determination of microbial carbon sources in petroleum contaminated sediments using molecular ^{14}C analysis. *Environ Sci Technol* 39(8):2552–2558.
34. Leahy JG, Colwell RR (1990) Microbial degradation of hydrocarbons in the environment. *Microbiol Rev* 54(3):305–315.
35. Grossi V, Massias D, Stora G, Bertrand J-C (2002) Burial, exportation and degradation of acyclic petroleum hydrocarbons following a simulated oil spill in bioturbated Mediterranean coastal sediments. *Chemosphere* 48(9):947–954.
36. Prince RC, et al. (1994) 17.α.(H)-21.β.(H)-hopane as a conserved internal marker for estimating the biodegradation of crude oil. *Environ Sci Technol* 28(1):142–145.
37. Venosa AD, Suidan MT, King D, Wrenn BA (1997) Use of hopane as a conservative biomarker for monitoring the bioremediation effectiveness of crude oil contaminating a sandy beach. *J Ind Microbiol Biotechnol* 18(2–3):131–139.
38. Demortier L, Lyons L (2002) Everything you always wanted to know about pulls. CDF Note 5776, version 2.10. Available at inspirehep.net/record/1354911/files/. Accessed June 14, 2016.
39. Douglas GS, Hardenstine JH, Liu B, Uhler AD (2012) Laboratory and field verification of a method to estimate the extent of petroleum biodegradation in soil. *Environ Sci Technol* 46(15):8279–8287.
40. Douglas GS, Owens EH, Hardenstine J, Prince RC (2002) The OSSA II pipeline oil spill: The character and weathering of the spilled oil. *Spill Sci Technol Bull* 7(3):135–148.
41. Heitkamp MA, Cerniglia CE (1987) Effects of chemical structure and exposure on the microbial degradation of polycyclic aromatic hydrocarbons in freshwater and estuarine ecosystems. *Environ Toxicol Chem* 6(7):535–546.
42. Wammer KH, Peters CA (2005) Polycyclic aromatic hydrocarbon biodegradation rates: A structure-based study. *Environ Sci Technol* 39(8):2571–2578.
43. Bossert ID, Bartha R (1986) Structure-biodegradability relationships of polycyclic aromatic hydrocarbons in soil. *Bull Environ Contam Toxicol* 37(4):490–495.
44. Wardlaw GD, Nelson RK, Reddy CM, Valentine DL (2011) Biodegradation preference for isomers of alkylated naphthalenes and benzothiophenes in marine sediment contaminated with crude oil. *Org Geochem* 42(6):630–639.
45. Aeppli C, et al. (2014) Recalcitrance and degradation of petroleum biomarkers upon abiotic and biotic natural weathering of Deepwater Horizon oil. *Environ Sci Technol* 48(12):6726–6734.
46. Overton EB, Miles MS, Meyer BM, Gao H, Turner RE (2014) Oil source fingerprinting in heavily weathered residues and coastal marsh samples. Proceedings of the International Oil Spill Conference 2014(1):2074–2082.
47. White HK, et al. (2012) Impact of the Deepwater Horizon oil spill on a deep-water coral community in the Gulf of Mexico. *Proc Natl Acad Sci USA* 109(50):20303–20308.
48. Stout S (2016) Oil spill fingerprinting method for oily matrices used in the Deepwater Horizon NRDA. *Environ Forensics* 17(3):218–243.
49. Frontera-Suau R, Bost FD, McDonald TJ, Morris PJ (2002) Aerobic biodegradation of hopanes and other biomarkers by crude oil-degrading enrichment cultures. *Environ Sci Technol* 36(21):4585–4592.
50. Carls MG, Holland L, Irvine GV, Mann DH, Lindeberg M (2016) Petroleum biomarkers as tracers of Exxon Valdez oil. *Environ Toxicol Chem* 35(11):2683–2690.
51. Short JW, et al. (2007) Slightly weathered Exxon Valdez oil persists in Gulf of Alaska beach sediments after 16 years. *Environ Sci Technol* 41(4):1245–1250.
52. Del'Arco JP, de França FP (2001) Influence of oil contamination levels on hydrocarbon biodegradation in sandy sediment. *Environ Pollut* 112(3):515–519.
53. Swannell RP, Lee K, McDonagh M (1996) Field evaluations of marine oil spill bioremediation. *Microbiol Rev* 60(2):342–365.
54. Mason OU, et al. (2012) Metagenome, metatranscriptome and single-cell sequencing reveal microbial response to Deepwater Horizon oil spill. *ISME J* 6(9):1715–1727.
55. Aman ZM, Paris CB, May EF, Johns ML, Lindo-Atichati D (2015) High-pressure visual experimental studies of oil-in-water dispersion droplet size. *Chem Eng Sci* 127: 392–400.
56. Kleindienst S, et al. (2015) Chemical dispersants can suppress the activity of natural oil-degrading microorganisms. *Proc Natl Acad Sci USA* 112(48):14900–14905.
57. Prince RC, Coolbaugh TS, Parkerton TF (2016) Oil dispersants do facilitate biodegradation of spilled oil. *Proc Natl Acad Sci USA* 113(11):E1421–E1421.
58. Wang Z, et al. (2007) *Oil Spill Environmental Forensics*, eds Wang Z, Stout SA (Elsevier, Burlington, MA), pp 73–146.